3	Author list
4 5 6 7	Sam Vickery ^{1,2} , William D. Hopkins ³ , Chet C. Sherwood ⁴ , Steven J. Schapiro ^{3,5} , Robert D. Latzman ⁶ , Svenja Caspers ^{7,8,9} , Christian Gaser ^{10,11} , Simon B. Eickhoff ^{1,2} , Robert Dahnke ^{10,11,12*} , Felix Hoffstaedter ^{1,2*} (*equal contribution)
8 9 10	1 Institute of Systems Neuroscience, Medical Faculty, Heinrich-Heine-University, Düsseldorf, Germany.
11 12	2 Institute of Neuroscience and Medicine (INM-7) Research Centre Jülich, Jülich, Germany
13 14 15	3 Keeling Center for Comparative Medicine and Research, The University of Texas MD Anderson Cancer Center, Bastrop, Texas
16 17 18	4 Department of Anthropology and Center for the Advanced Study of Human Paleobiology, The George Washington University, Washington, DC, USA.
19 20	5 Department of Experimental Medicine, University of Copenhagen, Copenhagen, Denmark
21 22	6 Department of Psychology, Georgia State University, Atlanta, GA, USA
23 24	7 Institute of Neuroscience and Medicine (INM-1), Research Centre Jülich, Jülich, Germany
25 26	8 Institute for Anatomy I, Medical Faculty, Heinrich-Heine-University, Düsseldorf, Germany
27 28	9 JARA-BRAIN, Jülich-Aachen Research Alliance, Jülich, Germany
29 30	10 Structural Brain Mapping Group, Department of Neurology, Jena University Hospital, Jena, Germany
31 32 33	11 Structural Brain Mapping Group, Department of Psychiatry and Psychotherapy, Jena University Hospital, Jena, Germany
34 35 36	12 Center of Functionally Integrative Neuroscience, Department of Clinical Medicine, Aarhus University, Denmark
37 38 39	
5)	

Chimpanzee Brain Morphometry Utilizing Standardized MRI Preprocessing

and Macroanatomical Annotations

41 Abstract

Chimpanzees are among the closest living relatives to humans and, as such, provide a crucial comparative model for investigating primate brain evolution. In recent years, human brain mapping has strongly benefited from enhanced computational models and image processing pipelines that could also improve data analyses in animals by using species-specific templates. In this study, we use structural MRI data from the National Chimpanzee Brain Resource (NCBR) to develop the chimpanzee brain reference template Juna. Chimp for spatial registration and the macro-anatomical brain parcellation Davi130 for standardized whole-brain analysis. Additionally, we introduce a ready-to-use image processing pipeline built upon the CAT12 toolbox in SPM12, implementing a standard human image preprocessing framework in chimpanzees. Applying this approach to data from 178 subjects, we find strong evidence for age-related GM atrophy in multiple regions of the chimpanzee brain, as well as, a human-like anterior-posterior pattern of hemispheric asymmetry in medial chimpanzee brain regions.

56 Introduction

5758

59

60

6162

63

64

65

66

67

68 69

70

71

72

73

74

75

76

77

78

79

80

81

82

83

84

85

Chimpanzees (Pan troglodytes) along with bonobos (Pan paniscus) represent the closest extant relatives of humans sharing a common ancestor approximately 7-8 million years ago (Langergraber et al. 2012). Experimental and observational studies, in both the field and in captivity, have documented a range of cognitive abilities that are shared with humans such as tool use and manufacturing (Shumaker et al. 2011), symbolic thought (de Waal 1996), mirror self-recognition (Anderson and Gallup 2015; Hecht et al. 2017) and some basic elements of language (Savage-Rumbaugh 1986; Savage-Rumbaugh and Lewin 1994; Tomasello and Call 1997) like conceptual metaphorical mapping (Dahl and Adachi 2013). This cognitive complexity together with similar neuroanatomical features (Zilles et al. 1989; Rilling and Insel 1999; Gomez-Robles et al. 2013; Hopkins et al. 2014a, 2017) and genetic proximity (Waterson et al. 2005) renders these species unique among non-human primates to study the evolutional origins of the human condition. In view of evolutionary neurobiology, the relatively recent divergence between humans and chimpanzees explains the striking similarities in major gyri and sulci, despite profound differences in overall brain size. Numerous studies using magnetic resonance imaging (MRI) have compared relative brain size, shape, and gyrification in humans and chimpanzees (Zilles et al. 1989; Rilling and Insel 1999; Gomez-Robles et al. 2013; Hopkins et al. 2014b, 2017).

Previous studies of brain aging in chimpanzees have reported minimal indications of atrophy (Herndon et al. 1999; Sherwood et al. 2011; Chen et al. 2013; Autrey et al. 2014). Nevertheless, Edler and colleagues (2017) recently found that brains of older chimpanzees' exhibit both neurofibrillary tangles and amyloid plaques, the classical features of Alzheimer's disease (AD). Neurodegeneration in the aging human brain includes marked atrophy in frontal and temporal lobes and decline in glucose metabolism even in the absence of detectable amyloid beta deposition, which increases the likelihood of cognitive decline and development of AD (Jagust 2018). Given the strong association of brain atrophy and amyloid beta in humans, this phenomenon requires further investigation in chimpanzees.

Cortical asymmetry is a prominent feature of brain organization in many primate species (Hopkins et al. 2015) and was recently shown in humans in a large scale ENIGMA (Enhancing Neuroimaging Genetics through Meta-Analysis) study (Kong et al. 2018). For chimpanzees, various studies have reported population-level asymmetries in different parts of the brain associated with higher order cognitive functions like tool-use (Freeman et al. 2004; Hopkins et al. 2008, 2017; Hopkins and Nir 2010; Lyn et al. 2011; Bogart et al. 2012; Gilissen and Hopkins 2013) but these results are difficult to compare within and across species, due to the lack of standardized registration and parcellation techniques as found for humans.

To date, there is no common reference space for the chimpanzee brain available to reliably associate and quantitatively compare neuro-anatomical evidence, nor is there a standardized image processing protocol for T1-weighted brain images from chimpanzees that matches human imaging standards. With the introduction of voxel-based morphometry (VBM, Ashburner and Friston 2000) and the ICBM (international consortium of brain mapping) standard human reference brain templates almost two decades ago (Mazziotta et al. 2001) MRI analyses became directly comparable and generally reproducible In this study we adapt state-of-the-art MRI (magnetic resonance imaging) processing methods to assess brain aging and cortical asymmetry in the chimpanzee brain. To make this possible, we rely on the largest openly available resource of chimpanzee MRI data: the *National Chimpanzee Brain Resource* (NCBR, <u>www.chimpanzeebrain.org</u>), including in vivo MRI images of 223 subjects from 9 to 54 years of age (Mean age = 26.9) ± 10.2 years). The aim of this study is the creation of a chimpanzee template permitting automated and reproducible image registration, normalization, statistical analysis and visualization to systematically investigate brain aging and hemispheric asymmetry in chimpanzees.

112 Results

Initially, we created the population based Juna (Forschungszentrum <u>Juelich</u> - University Je<u>na</u>) T1-template, tissue probability maps (TPM) for tissue classification and a non-linear spatial registration 'Shooting' templates (Figure 1) in an iterative fashion at 1mm spatial resolution. The preprocessing pipeline and templates creation were established using the freely available *Statistical Parametric Mapping* (SPM12 v7487, http://www.fil.ion.ucl.ac.uk/spm/) software and *Computational Anatomy Toolbox* (CAT12 r1434, http://www.neuro.uni-jena.de/cat/). Juna.Chimp templates and the Davi130 parcellation as well as images for analysis are interactively accessible via the Juna.Chimp web viewer (http://junachimp.inm7.de/).

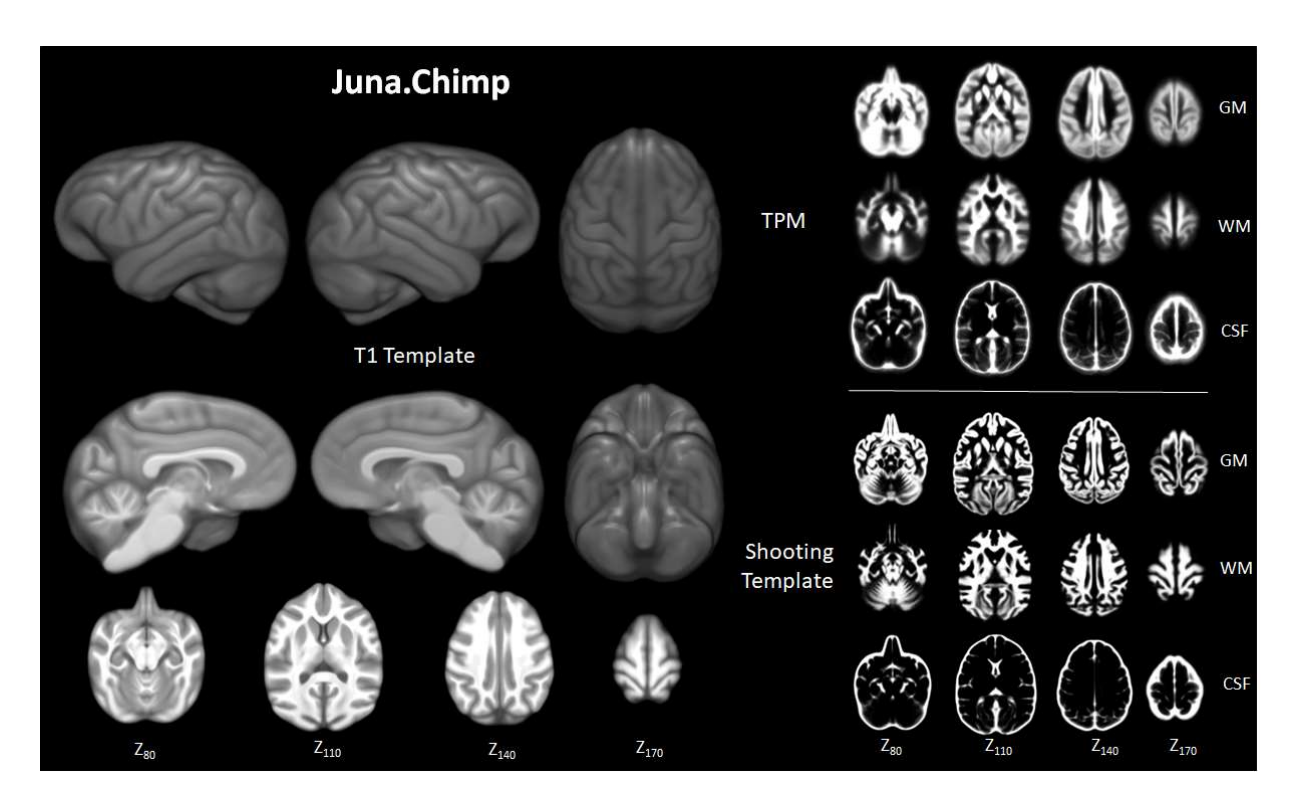


Figure 1. Juna.Chimp templates including the average T1- template, tissue probability maps (TPM), and Geodesic Shooting template. For Shooting templates and TPM axial slices are shown of gray matter (GM), white matter (WM), and cerebrospinal fluid (CSF). All templates are presented at 0.5mm resolution.

To enable more direct comparison to previous research, we manually created the Davi130 parcellation (by R.D. and S.V.), a whole brain macroanatomical annotation

based on the Juna T1 template (Figure 2). The delineation of regions within the cortex was determined by following major gyri and sulci, whereby, large regions were arbitrarily split into two to three sub-regions of approximate equal size even though histological studies show that micro-anatomical borders between brain regions are rarely situated at the fundus (Sherwood et al. 2003; Schenker et al. 2010; Spocter et al. 2010; Amunts and Zilles 2015).. This process yielded 65 regions per hemisphere for a total of 130 regions for the Davi130 macro-anatomical manual parcellation (Figure 2 and Figure 2 – source data 1).

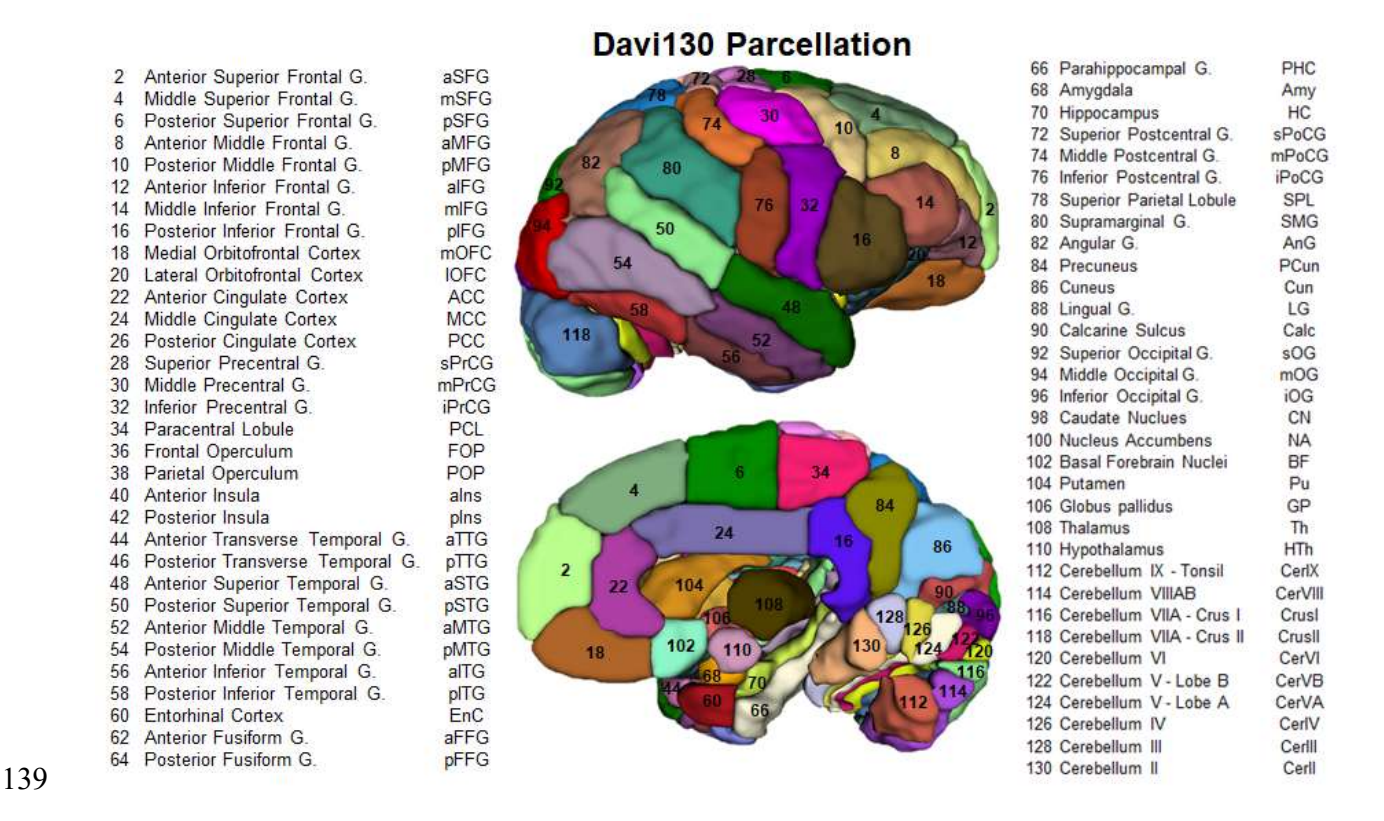


Figure 2. Lateral and medial aspect of the Davi130 parcellation right hemisphere. Visible regions are numbered with Davi130 parcellation region numbers and correspond to names in the figure. Odd numbers correspond to left hemisphere regions while even numbers are in the right hemisphere. A list of all Davi130 labels can be found at Figure 2 – source data 1.

Following successful CAT12 preprocessing rigorous quality control (QC) was employed to identify individual MRI scans suitable for statistical analysis of brain aging and hemispheric asymmetry in chimpanzees. Our final sample consists of 178 chimpanzees

including 120 females with an age range of 11 to 54 years and a mean age of 26.7 ± 9.8 years (Figure 3A). Correlation analysis between GM fraction of total intracranial volume and age revealed a significant negative association between the two ($R^2 = 0.11$, p < 0.0001) demonstrating age-related decline in overall GM (Figure 3B). Both male and female subjects show a significant age effect on GM (male: $R^2 = 0.08$, p = 0.03; female $R^2 = 0.11$, p = 0.0001). The linear model showed no significant sex differences of GM decline (p = 0.08).

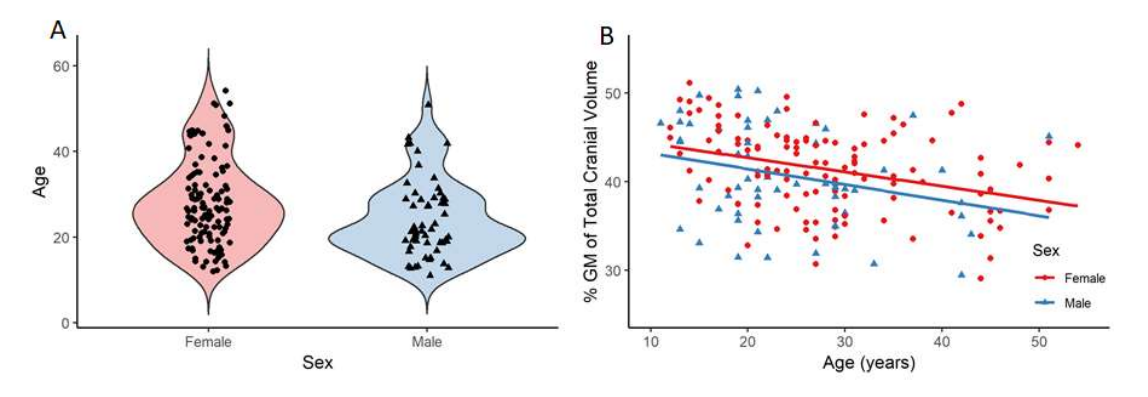


Figure 3. A - Distribution of age and sex in the final sample of 178 chimpanzees. B- linear relationship between GM and age for female and male respectively. Figure 1 – figure supplement 1 presents the age and sex distribution of the whole sample (n=223).

Region based morphometry analysis was applied to test for local effect of age on GM. Linear regression analyses identified 23 regions in the Davi130 parcellation across both hemispheres that were significantly associated with age after family-wise error (FWE) correction for multiple testing (Figure 4, for all region results see Supplementary). Specifically, GM decline with age was found bilaterally in the lateral orbitofrontal cortex (IOFC) and mid-cingulate (MCC) as well as unilaterally in the right precuneus (PCun), posterior cingulate (PCC), and lingual gyrus (LG), in addition to the left middle superior frontal gyrus(mSFG), anterior transverse temporal gyrus (aTTG) and calcarine sulcus (Calc) within the cerebral cortex. The strongest association with aging was in the bilateral putamen (Pu) and caudate nucleus (CN), while the nucleus accumbens (NA) and superior cerebellum (CerIII, CerIV, CerVA, and right CrusII) also presented a significant aging effect. Finally, to test for more fine grained effects of aging, the same sample was analyzed with VBM revealing additional clusters of GM that are significantly affected by age in chimpanzees (Figure 5)

after FWE correction using threshold-free cluster enhancement (TFCE) (Smith and Nichols 2009). On top of the regions identified by region-wise morphometry, we found voxel-wise effects throughout anterior cingulate cortex (ACC), middle frontal gyrus (MFG) and in parts of the superior and inferior frontal gyrus (SFG, IFG), postcentral gyrus, superior and transverse temporal gyrus (STG, TTG), angular gyrus (AnG), superior occipital gyrus (sOG) and in inferior parts of the cerebellum.

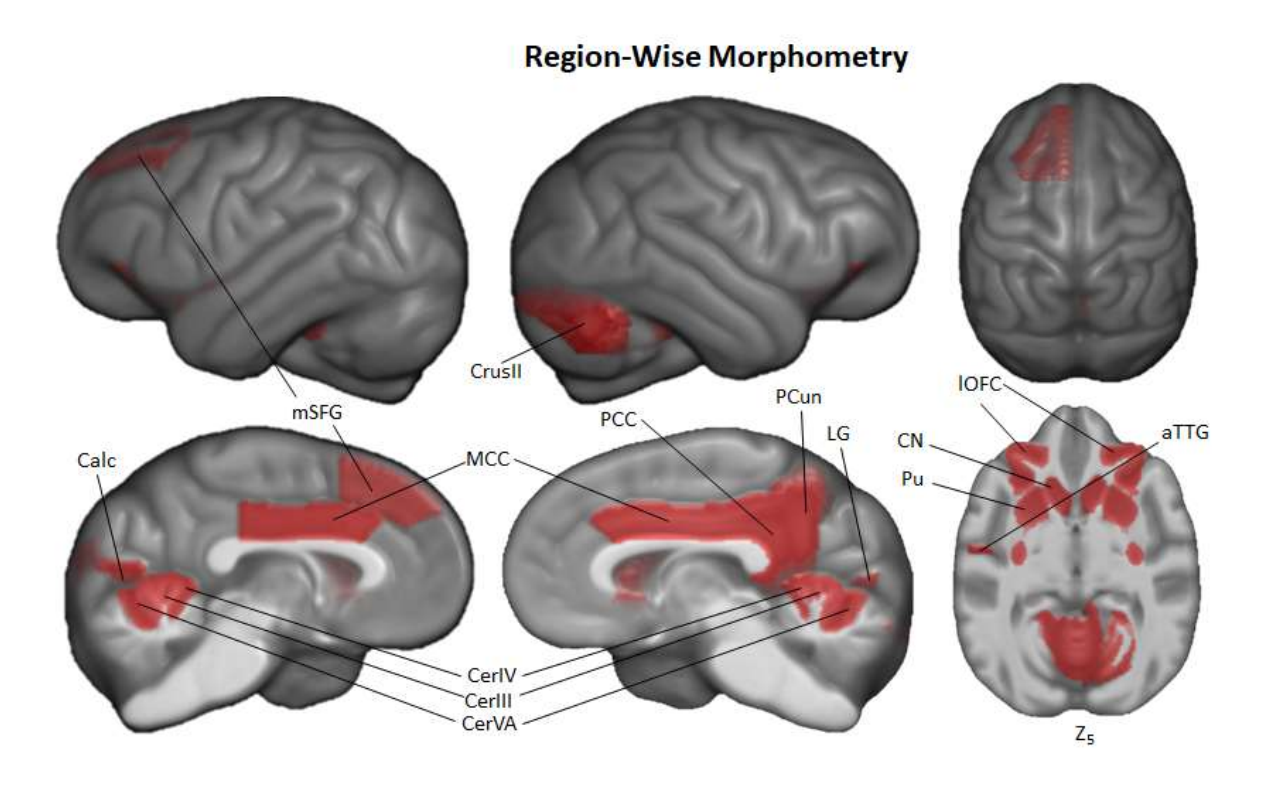


Figure 4. Region-wise morphometry in the Davi130 parcellation age regression where red regions represent Davi130 regions that remained significant at $p \le 0.05$ following FWE correction. The T-statistic and p-value for all Davi130 labels can be found in Figure 4 − source data 1. aTTG − anterior transverse temporal gyrus, Calc − Calcarine sulcus, CrusII − cerebellum VIIA-CrusII, CerVA − cerebellum VA, CerIV − cerebellum IV, CerIII − cerebellum III, CN − caudate nucleus, IOFC − lateral orbitofrontal cortex, LG − lingual gyrus, MCC − medial cingulate cortex, mSFG − middle superior frontal gyrus, PCC − posterior cingulate cortex, PCun − precuneus, Pu − putamen.

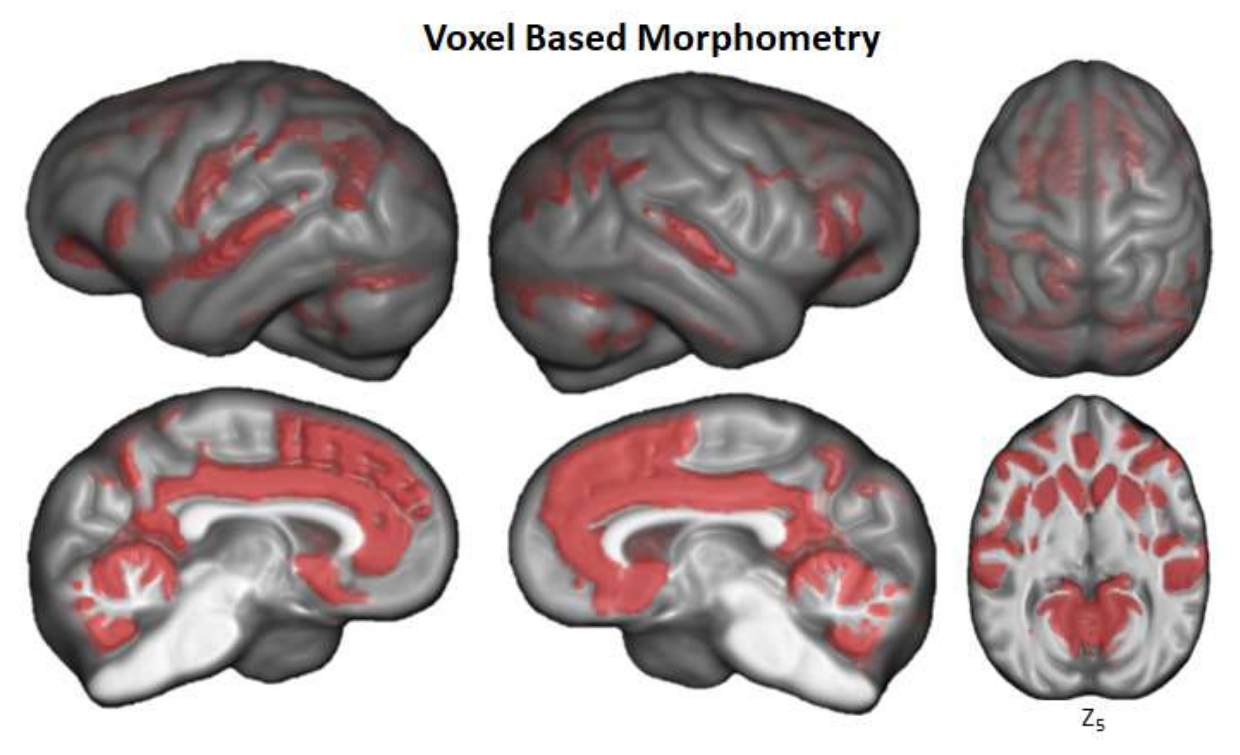


Figure 5. Voxel based morphometry of aging on GM volume using TFCE with FWE correction at $p \le 0.05$.

Hemispheric asymmetry of the chimpanzee brain was assessed for each cortical Davi130 region with a total of 29 macro-anatomical regions exhibiting significant cortical asymmetry after FWE correction (Figure 6, all region asymmetry found in Supplementary). Slightly more regions were found with greater GM volume on the right hemisphere (n=17) as compared to the left (n=12). In the left hemisphere, we found more GM laterally in the inferior postcentral gyrus (iPoCG), supramarginal gyrus (SMG) and superior occipital gyrus (sOG), insula and posterior TTG as well as medially in the orbitofrontal cortex (mOFG), basal forebrain nuclei (BF), hippocampus (HC), and anterior SFG. Rightward cortical asymmetry was located medially in the paracentral lobule (PCL), PCC, cuneus (Cun) and the region surrounding the calcarine sulcus, in the parahippocampal gyrus (PHC) and posterior fusiform gyrus (pFFG), as well as in the parietal operculum (POP). Laterally, rightward cortical asymmetry was found in the middle postcentral gyrus (mPoCG) and posterior superior temporal gyrus (pSTG). Within the basal ganglia, leftward GM asymmetry was observed in the putamen (Pu) while, rightward asymmetry is in the globus pallidus (GP) and thalamus (Th). In the anterior cerebellar lobe, there was

leftward (CerIV) and rightward (CerII) GM asymmetry. The posterior cerebellum showed only rightward (CerVI, CerVB, and CerIX) asymmetry.

The moderate pattern of asymmetry we observed medially was a shift from more anterior regions showing leftward GM asymmetry (mOFC, BF, and aSFG) while more posterior regions presented rightward asymmetry (PCL, PCC, Cun, Calc, and LG). The lateral regions did not show a decipherable pattern.

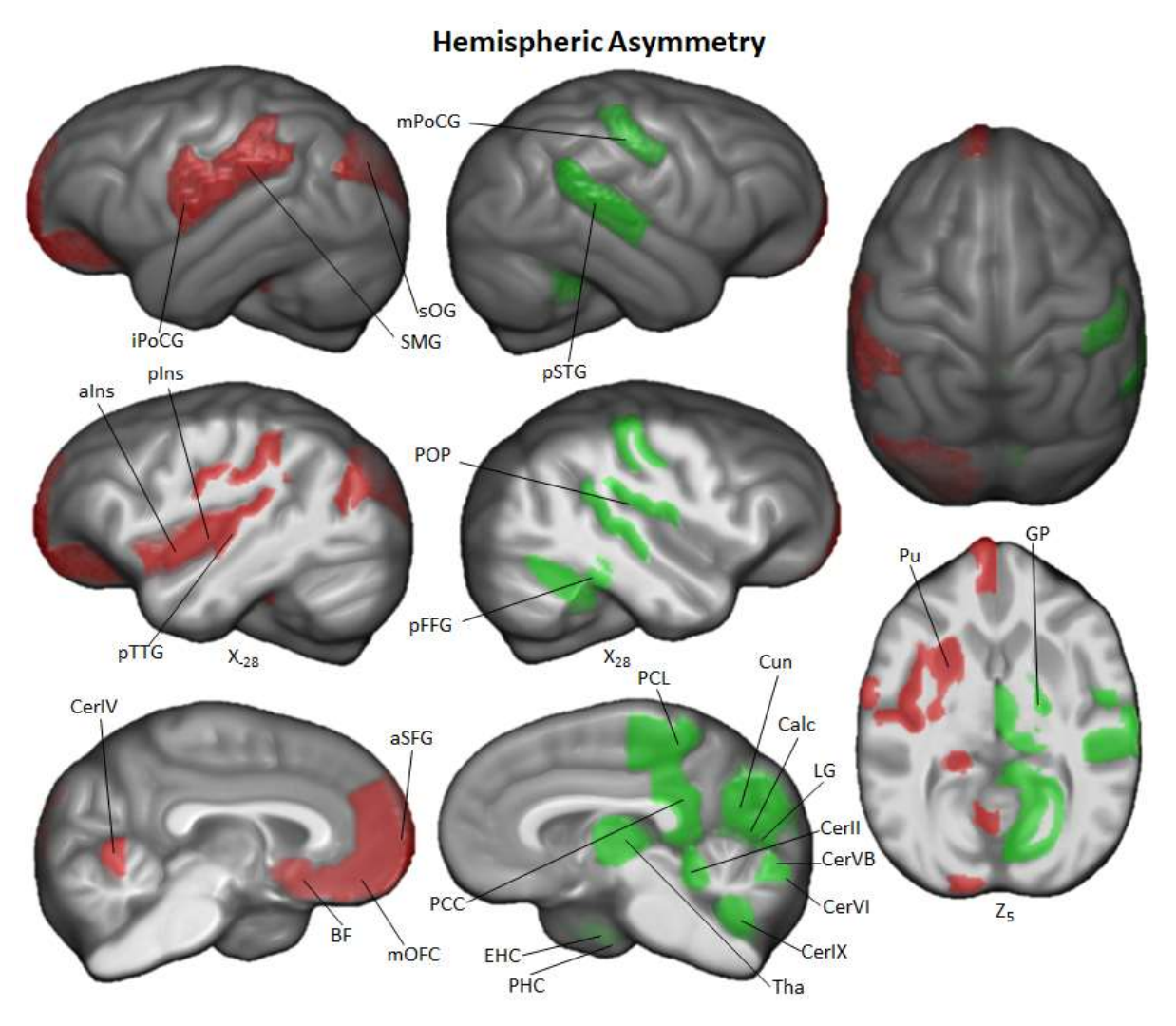


Figure 6. Hemispheric asymmetry of Davi130 regions within the chimpanzee sample. Significant leftward (red) and rightward (green) asymmetrical regions are those with a $p \le 0.05$ after FWE correction. The T-statistic and p-value for all Davi130 labels can be found in Figure 6 – source

data 1. alns – anterior insula, aSFG – anterior superior frontal gyrus, BF – basal forebrain nuclei, Calc – calcarine sulcus, CerlX – cerebellum IX, CerVB – cerebellum V anterior B, CerVI – cerebellum VI, CerlV – cerebellum IV, CerlI, cerebellum II, Cun – cuneus, EnC – entorhinal cortex, GP – globus pallidus, iPoCG – inferior postcentral gyrus, LG – lingual gyrus, mOFC – medial orbitofrontal cortex, mPoCG – middle postcentral gyrus, PCC – posterior cingulate cortex, PCL – paracentral lobule, pFFG – posterior fusiform gyrus, PHC – parahippocampal gyrus, pIns – posterior insula, POP – parietal operculum, pSTG – posterior superior temporal gyrus, pTTG – posterior transverse temporal gyrus, Pu – putamen, SMG – supramarginal gyrus, sOG – superior occipital gyrus, Th – thalamus. The hippocampus (HC) is significantly leftward lateralized but is not shown in this figure.

228 Discussion

As a common reference space for the analysis of chimpanzee brain data, we created the Juna. Chimp template, constructed from a large heterogeneous sample of T1-weighted MRI's from the NCBR. The Juna. Chimp template includes a reference T1-template, along with probability maps of brain and head tissues accompanied by a Geodesic Shooting template for the publicly available SPM12/CAT12 preprocessing pipeline to efficiently segment and spatially normalize individual chimpanzee T1 images. The T1-template and TPM can be also used as the target for image registration with other popular software packages, such as FSL (https://fsl.fmrib.ox.ac.uk/fsl) or ANTs (https://fsl.fmrib.ox.ac.uk/fsl).

Additionally, we provide the manually segmented, macro-anatomical Davi130 whole-brain parcellation comprising 130 cortical, sub-cortical and cerebellar brain regions, which enables systematical extraction of volumes-of-interest from chimpanzee MRI data. The image processing pipeline and Davi130 parcellation were used to investigate ageing and interhemispheric asymmetry in the chimpanzee brain. Our analyses demonstrated strong age-related GM atrophy as well as marked hemispheric asymmetry over the whole cortex.

We found clear evidence of global and local GM decline in the aging chimpanzee brain even though previous research into age-related changes in chimpanzee brain organization has shown little to no effect (Herndon et al. 1999; Sherwood et al. 2011; Chen et al. 2013; Autrey et al. 2014). This can be attributed on the one hand to the larger number of MRI scans available via the NCBR including 30% of older subjects with 55 individuals over 30 and 12 over 45 years of age, which is crucial for modelling the effect of aging (Chen et al. 2013; Autrey et al. 2014). On the other hand, state-of-the-art image processing enabled the creation of the species specific Juna. Chimp templates, which largely improves tissue segmentation and registration accuracy (Ashburner and Friston 2000). Non-linear registration was also improved by the large heterogeneous sample utilized for the creation of the templates encompassing a representative amount of inter-individual variation. We used the well-established structural brain imaging toolbox CAT12 to build a reusable chimpanzee preprocessing pipeline catered towards analyzing local tissue-specific anatomical variations as measured with T1 weighted MRI. The Davi130-based region-wise and the voxel-wise morphometry analysis consistently showed localized GM decline in IOFC, the basal ganglia, MCC, PCC, PCun and superior cerebellum. The VBM approach additionally produced evidence for age effects in bilateral prefrontal cortex, ACC, superior temporal regions and throughout the cerebellum. These additional effects can be expected, as VBM is more sensitive to GM changes due to aging (Kennedy et al. 2009). The brain regions revealing GM decline in both approaches in particular medial and temporal cortical regions and the basal ganglia have also been shown to exhibit GM atrophy during healthy aging in humans (Good et al. 2001b; Kennedy et al. 2009; Crivello et al. 2014; Minkova et al. 2017).

245

246247

248

249

250

251

252

253

254

255

256

257

258

259

260

261

262

263

264265

266

267

268

269

270

271

272

273

274

275

Very recently, it has been shown that stress hormone levels increase with age in chimpanzees, a process previously thought to only occur in humans which can cause GM volume decline (Emery Thompson et al. 2020). This further strengthens the argument that age-related GM decline is also shared by humans closest relative, the chimpanzee. Furthermore, Edler et al. (2017) found Alzheimer's disease-like accumulation of amyloid beta plaques and neurofibrillary tangles located predominantly in prefrontal and temporal cortices in a sample of elderly chimpanzees between 37 and 62 years of age. As the aggregation of these proteins is associated with localized neuronal loss and cortical atrophy in

humans (La Joie et al. 2012; Llado et al. 2018), the age-related decline in GM volume shown here is well in line with the findings by Jagust (2016) associating GM atrophy with amyloid beta. These findings provide a biological mechanism for accelerated GM decrease in prefrontal, limbic, and temporal cortices in chimpanzees. In contrast, elderly rhesus monkeys show GM volume decline without the presence of neurofibrillary tangles (Alexander et al. 2008; Shamy et al. 2011). Taken together, regionally specific GM atrophy seems to be a common aspect of the primate brain aging pattern observed in macaque monkeys, chimpanzees and humans. Yet, to make a case for the existence of Alzheimer's disease in chimpanzees, validated cognitive tests for Alzheimer's-like cognitive decline in non-human primates are needed, to test for direct associations between cognitive decline with tau pathology and brain atrophy.

Hemispheric asymmetry was found in almost two-thirds of all regions of the Davi130 parcellation, reproducing several regional findings reported in previous studies using diverse image processing methods as well as uncovering numerous novel population-level asymmetries. Previous studies utilizing a region-wise approach based on handdrawn or atlas derived regions also reported leftward asymmetry of volume of the planum temporale (PT) (Lyn et al. 2011; Gilissen and Hopkins 2013), and of cortical thickness in STG (Hopkins and Avants 2013), and the insula (Hopkins et al. 2017). Region-wise morphometry also demonstrated rightward asymmetry in thickness of the PCL and PHC (Hopkins et al. 2017). Previous VBM findings also revealed leftward asymmetry in the anterior SFG and SMG along with rightward lateralization of the posterior SFG, and middle part of the PoCG (Hopkins et al. 2008). In the current study, new regions of larger GM volume in the left hemisphere were found in frontal (mSFG, mOFC), limbic (HC), temporal (aTTG), and parietal (iPoCG) cortices as well as in the basal ganglia (BF, Pu) and cerebellum (CerlV). Novel rightward asymmetries could also be seen in temporal (pFFG). limbic (PCC, EnG), parietal (POP), and occipital (Cun, LG, Calc) cortices besides the basal ganglia (Th, GP) and the cerebellum (CerlX, CerVI, CerVB, CerII).

Significant leftward asymmetries in Davi130s' region pTTG which contains the PT, is consistent with previous studies in GM volume of the PT, its surface area (Hopkins and Nir 2010), and cytoarchitecture (Zilles et al. 1996; Gannon et al. 1998; Spocter et al.

2010). At this cortical location, old world monkeys lack the morphological features of the PT, nevertheless several species have been shown to display asymmetry in Sylvian fissure length (Lyn et al. 2011; Marie et al. 2018).

Interestingly, the parietal operculum showed rightward asymmetry, while Gilissen and Hopkins (2013) showed that the left parietal operculum was significantly longer in chimpanzees, compared to the right. The left lateral sulcus in the Juna. Chimp template appears to proceed further posteriorly and superiorly compared to the right, confirming this finding, even though we found greater GM volume in the right POP as compared to the left.

Population-level asymmetries in the pIFG in chimpanzees were documented almost two decades ago by Cantalupo and Hopkins (2001), who reported a leftward asymmetry in pIFG volume in a small sample of great apes. In subsequent studies this result could not be replicated when considering GM volume (Hopkins et al. 2008; Keller et al. 2009) or cytoarchitecture (Schenker et al. 2010). We also failed to find a leftward asymmetry in GM volume for the pIFG, in contrary to asymmetries found in humans (Amunts et al. 1999; Uylings et al. 2006; Keller et al. 2009). The prominent leftward PT asymmetry in chimpanzees is also a well-documented population-level asymmetry in humans (Good et al. 2001a; Watkins 2001). The overall regional distribution of asymmetry in chimpanzees is partially similar to that found in human cortical organization (Good et al. 2001a; Luders et al. 2006; Zhou et al. 2013; Koelkebeck et al. 2014; Plessen et al. 2014; Chiarello et al. 2016; Maingault et al. 2016; Kong et al. 2018).

Gross hemispheric asymmetry in humans follows a general structure of frontal rightward and occipital leftward asymmetry known as the 'Yakovlevian torque'. This refers to the bending of the anterior right hemisphere over the midline into the left and the posterior left hemisphere bending over to the right and is represented as differences in widths of frontal and occipital lobes (Toga and Thompson 2003). This organizational trait was apparent in the Juna. Chimp templates with a slight frontal and occipital bending, which was manually adapted when labelling the medial Davi130 regions. The higher leftward GM density in frontal regions and rightward asymmetry in occipital regions may also follow

this trend. Of note, this organizational pattern of asymmetry was less apparent in lateral cortical structures, however medially, this anterior-posterior asymmetry is evident in chimpanzees, challenging recent findings from Li and colleagues (2018) who rejected the 'Yakovlevian torque' in chimpanzees. Specifically, leftward asymmetry of the frontal regions aSFG, BF, and mOFC and the rightward asymmetry of posterior regions PCL, PCC, Cun, Calc, and LG aligns with the pattern of asymmetry reported in human cortical GM volume, thickness and surface area (Luders et al. 2006; Zhou et al. 2013; Plessen et al. 2014; Chiarello et al. 2016; Kong et al. 2018).

The NCBR offers the largest and richest openly available dataset of chimpanzee brain MRI scans acquired over a decade with 1.5T and 3T MRI at two locations, capturing valuable inter-individual variation in one large heterogeneous sample. To account for the scanner effect on GM estimation, field strength was modelled as a covariate of no interest for analyzing the age effect on GM volume. Rearing has been shown to affect GM structural covariance networks and cortical organization (Bogart et al. 2014; Bard and Hopkins 2018) while handedness has been shown to correlate with asymmetry in the motor cortex (Hopkins and Cantalupo 2004) and the volume of IFG (Taglialatela et al. 2006) as well as with gyrification asymmetry (Hopkins et al. 2007). Therefore, these covariates may also modulate hemispheric asymmetry and/or age-related GM volume decline here, but as these data were not available for all subjects, we did not consider these effects in order to include as many subjects as possible to model effects of age. The focus of this study was the analysis of GM volume, even though the CAT12 image processing pipeline includes surface projection and analysis. Consequently, the next step will be the application of CAT12 to analyze cortical surface area, curvature, gyrification, and thickness of the chimpanzee brain, to include behavioral data and the quantitative comparison to humans and other species, as cortical surface projection permits a direct inter-species comparison due to cross species registration.

361

363

364

335

336

337

338

339

340

341

342

343

344

345

346

347

348

349

350

351

352

353

354

355

356

357

358

359

360

362 Conclusion

In conclusion, we present the new chimpanzee reference template Juna. Chimp, TPM's, the Davi130 whole brain parcellation, and the CAT12 preprocessing pipeline

which is ready-to-use by the wider neuroimaging community. Investigations of age-related GM changes in chimpanzees using both region-wise and voxel-based morphometry, showed a substantial age effect, providing further evidence for human like physiological aging processes in chimpanzees. Examining population based cortical asymmetry in chimpanzees yielded further evidence for the well-documented lateralization of PT. Additionally, an anterior-posterior left-right pattern of asymmetry as observed in humans was found predominantly in medial regions of the chimpanzee cortex.

372

373

374

375

376

377

378

379

380

381

382

383

384

385

386

387

388

389

390

365

366

367

368

369

370

371

Materials and Methods

Subject Information and Image Collection Procedure

This study analyzed structural T1-weighted MRI scans of 223 chimpanzees (137 females; 9 - 54 y/o, mean age 26.9 ± 10.2 years, Figure 3 – Supplementary figure 1) from the NCBR (www.chimpanzeebrain.org). The chimpanzees were housed at two locations including, the National Center for Chimpanzee Care of The University of Texas MD Anderson Cancer Center (UTMDACC) and the Yerkes National Primate Research Center (YNPRC) of Emory University. The standard MR imaging procedures for chimpanzees at the YNPRC and UTMDACC are designed to minimize stress for the subjects. For an indepth explanation of the imaging procedure please refer to Autrey et al. (2014). Seventysix chimpanzees were scanned with a Siemens Trio 3 Tesla scanner (Siemens Medical Solutions USA, Inc., Malvern, Pennsylvania, USA). Most T1-weighted images were collected using a three-dimensional gradient echo sequence with 0.6 × 0.6 × 0.6 resolution (pulse repetition = 2300 ms, echo time = 4.4 ms, number of signals averaged = 3). The remaining 147 chimpanzees were scanned using a 1.5T GE echo-speed Horizon LX MR scanner (GE Medical Systems, Milwaukee, WI), predominantly applying gradient echo sequence with $0.7 \times 0.7 \times 1.2$ resolution (pulse repetition = 19.0 ms, echo time = 8.5 ms, number of signals averaged = 8).

DICOM conversion and De-noising

391

392

393

394

395

396

397

398

399

400

401

402

403

404

405

406

407

408

409

410

411

412

413

414

415

416

417

418

The structural T1-weighted images were provided by the NCBR in their original DICOM format and converted into Nifti using MRIcron (Rorder and Brett 2000). If multiple scans were available, the average was computed. Following DICOM conversion each image was cleaned of noise (Manjon et al. 2010) and signal inhomogeneity and resliced to 0.6 mm isotropic resolution. Finally, the anterior commissure was manually set as the center (0,0,0) of all Nifti's to aid in affine preprocessing.

CAT12 Preprocessing Segmentation

Structural image segmentation in CAT12 builds on the TPM-based approach employed by SPM12, whereby, the gray/white image intensity is aided with a priori tissue probabilities in initial segmentation and affine registration as it is in common template space. Another advantage of a TPM is that one has a template for initial affine registration, which then enables the segment maps to be non-linearly registered and spatially normalized to corresponding segment maps of the chimpanzee shooting templates. Lowering the possibility for registration errors improves the quality of the final normalized image. Improving upon SPM's segmentation (Ashburner and Friston 2005), CAT12 employs Local Adaptive Segmentation (LAS) (Dahnke et al. 2012), Adaptive Maximum A Posterior segmentation(AMAP) (Dahnke and Gaser 2017; Gaser et al. 2020), and Partial Volume Estimation (PVE) (Tohka et al. 2004). LAS creates local intensity transformations for all tissue types to limit GM misclassification due to varying GM intensity in regions such as the occipital, basal ganglia, and motor cortex as a result of anatomical properties (e.g. high myelination and iron content). AMAP segmentation takes the initially segmented, aligned, and skull stripped image created utilizing the TPM and disregards the a priori information of the TPM, to conduct an adaptive AMAP estimation where local variations are modelled by slowly varying spatial functions (Rajapakse et al. 1997). Along with the classical three tissue types for segmentation (GM, WM, & CSF) based on the AMAP estimation, an additional two PVE classes (GM-WM & GM-CSF) are created resulting in an estimate of the fraction of each tissue type contained in each

voxel. These features outlined above of our pipeline allow for more accurate tissue segmentation and therefore a better representation of macroanatomical GM levels for analysis.

<u>Creation of Chimpanzee Templates</u>

419

420

421

422

423

424

425

426

427

428

429

430

431

432

433

434

435

436

437

438

439

440

441

442

443

An iterative process as by Franke et al. (2017) was employed to create the Juna. Chimp template, with T1 average, Shooting registration template (Ashburner and Friston 2011), as well as the TPM (Figure 7). Initially, a first-generation template was produced using the "greater ape" template delivered by CAT (Franke et al. 2017; Gaser et al. 2020) that utilizes data provided in Rilling and Insel (1999). The final segmentation takes the bias-corrected, intensity-normalized, and skull-stripped image together with the initial SPM-segmentation to conduct an AMAP estimation (Rajapakse et al. 1997) with a partial volume model for sub-voxel accuracy (Tohka et al. 2004). The affine normalized tissue segments of GM, WM, and CSF were used to create a new Shooting template that consists of four major non-linear normalization steps allowing to normalize new scans. To create a chimpanzee-specific TPM, we average the different Shooting template steps to benefit from the high spatial resolution of the final Shooting steps but also include the general affine aspects to avoid over-optimization. Besides the brain tissues the TPM also included two head tissues (bones and muscles) and a background class for standard SPM12 (Ashburner and Friston 2005) and CAT12 preprocessing. The internal CAT atlas was written for each subject and mapped to the new chimpanzee template using the information from the Shooting registration. The CAT atlas maps were averaged by a median filter and finally manually corrected. This initial template was then used in the second iteration of CAT segmentation to establish the final chimpanzee-specific Juna. Chimp template, which was imported into the standard CAT12 preprocessing pipeline to create the final data used for the aging and asymmetry analyses.

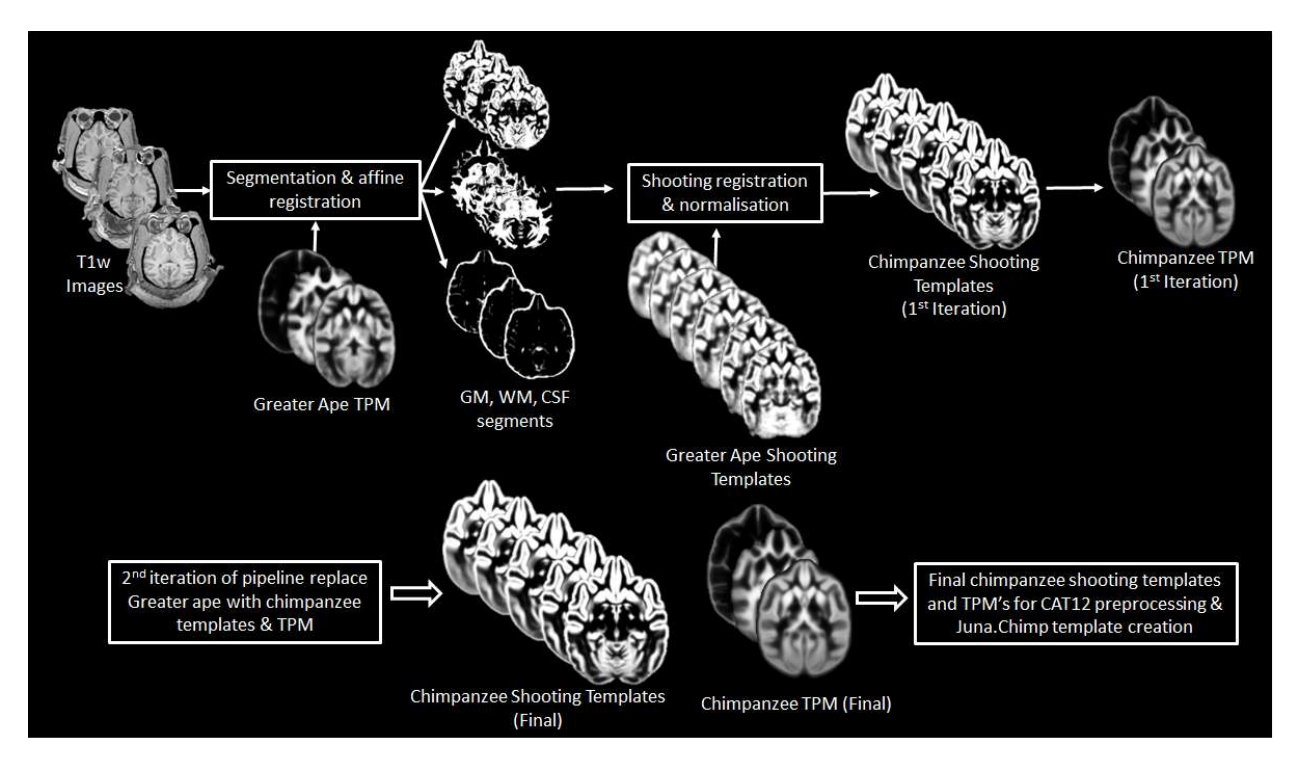


Figure 7. Workflow for creation of chimpanzee specific Shooting template and TPM, which can then be used in CAT12 structural preprocessing pipeline to create the Juna. Chimp template.

The resulting chimpanzee-Shooting template, TPM and CAT atlas establishes the robust and reliable base to segment and spatially normalize the T1-weighted images utilizing CAT12's processing pipeline (Dahnke and Gaser 2017; Gaser et al. 2020).

Davi130 parcellation

The average T1 and final Shooting template were used for a manual delineation of macro-anatomical GM structures. Identification and annotation of major brain regions were performed manually using the program, 3D Slicer 4.10.1 (https://www.slicer.org). The labeling enables automated, region-based analysis of the entire chimpanzee brain and allows for robust statistical analysis. Nomenclature and location of regions were ascertained by consulting both chimpanzee and human brain atlases (Bailey P, Bonin GV 1950; Mai et al. 2015). The labelling was completed by two authors (S.V. & R.D.) and reviewed by two experts of chimpanzee brain anatomy (C.C.S. & W.D.H.).

A total of 65 GM structures within the cerebrum and cerebellum of the left hemisphere were annotated and then flipped to the right hemisphere. The flipped annotations

were then manually adapted to the morphology of the right hemisphere to have complete coverage of the chimpanzee brain with 130 labels. The slight bending of the anterior part of the right hemisphere and the posterior part of the left hemisphere over the midline observed in our template and annotated within our Davi130 labelling, does not align with previous findings claiming that this morphological trait is specific to the human brain (Li et al. 2018; Xiang et al. 2019).

The location of macroscopic brain regions was determined based on major gyri of the cerebral cortex, as well as distinct anatomical landmarks of the cerebellar cortex, and basal ganglia. Of note, the border between two gyri was arbitrarily set as the mid-point of the connecting sulcus. Large gyri were further subdivided into two or three parts based on their size and structural features, such as sulcal fundi and gyral peaks, to enable greater spatial resolution and better inter-regional comparison. Naming of subdivisions was based entirely on spatial location, e.g., anterior, middle, posterior, and do not claim to correspond to functional parcellations.

Quality Control

CAT12 provides quality measures pertaining to noise, bias inhomogeneities, resolution and an overall compounded score of the original input image. Using these ratings, poor images were flagged for visual inspection when they were 2 standard deviations (std) away from the sample mean of each rating. The preprocessed modulated GM maps were then tested for sample inhomogeneity separately for each scanner (3T & 1.5T) and those that have a mean correlation below 2 std were flagged for visual inspection. Once the original image was flagged, affine GM, and modulated GM maps were inspected for poor quality, tissue misclassification, artefacts, irregular deformations, and very high intensities. For the second iteration, the passed modulated GM maps were tested again for mean correlation as a complete sample, flagging the images below 3 std for visual inspection. Looking for the same features as in the initial QC iteration. Following the two iterations of QC a total of 178 of 223 chimpanzee MRI's (120 females, 11 - 54 y/o, mean = 26.7 ± 9.8) qualified for statistical analysis.

Age-Related Changes in Total Gray Matter

A linear regression model was used to determine the effect of aging on total GM volume. Firstly, total GM volume for each subject was converted into a percentage of total intracranial volume (TIV) to account for the variation in head size. This was then entered into a linear regression model as the dependent variable with age and sex as the independents. Sex-specific models were conducted with males and females separately using age as the only dependent variable. The slope of each regression line was determined using R^2 and a p-value of $p \le 0.05$ was used to determine the significant effect of age and sex on total GM volume.

Age-Related Changes in Gray Matter Using Davi130 Parcellation

The Davi130 parcellation was applied to the modulated GM maps to conduct region-wise morphometry analysis. First, the Davi130 regions were masked with a 0.1 GM mask to remove all non-GM portions of the regions. Subsequently, the average GM intensity of each region for all QC-passed chimpanzees was calculated. A multiple regression model was conducted for the labels from both hemispheres, whereby, the dependent variable was GM volume and the predictor variables were age, sex, TIV, and scanner. Significant age-related GM decline was established for a Davi130 label with a $p \le 0.05$, after correcting for multiple comparisons using FWE (Holm 1979).

Voxel-Based Morphometry

VBM analysis was conducted using CAT12 to determine the effect of aging on local GM volume. The modulated and spatially normalized GM segments from each subject were spatially smoothed with a 4 mm FWHM (full width half maximum) kernel prior to analyses. To restrict the overall volume of interest, an implicit 0.4 GM mask was employed. As MRI field strength is known to influence image quality, and consequently, tissue classification, we included scanner strength in our VBM model as a covariate. The dependent variable in the model was age, with covariates of TIV, sex, and scanner. The VBM model was corrected for multiple comparisons using TFCE with 5000 permutations

(Smith and Nichols 2009). Significant clusters were determined at $p \le 0.05$, after correcting for multiple comparisons using FWE.

Hemispheric Asymmetry

As for the age regression analysis, all Davi130 parcels were masked with a 0.1 GM mask to remove non-GM portions within regions. Cortical hemispheric asymmetry of Davi130 labels was determined using the formula Asym = (L - R) / (L + R) * 0.5 (Kurth et al. 2015; Hopkins et al. 2017), whereby L and R represent the average GM volume for each region in the left and right hemisphere, respectively. Therefore, the bi-hemispheric Davi130 regions were converted into single Asym labels (n=65) with positive Asym values indicating a leftward asymmetry, and negative values, a rightward bias. One-sample t-tests were conducted for each region under the null hypothesis of Asym = 0, and significant leftward or rightward asymmetry was determined with a $p \le 0.05$, after correcting for multiple comparisons using FWE (Holm 1979).

Exemplar Pipeline Workflow

To illustrate the structural processing pipeline, we have created exemplar MATLAB SPM batch scripts that utilizes the Juna. Chimp templates in CAT12's preprocessing workflow to conduct segmentation, spatial registration, and finally some basic age analysis on an openly available direct-to-download chimpanzee sample (http://www.chimpanzee-brain.org/mri-datasets-for-direct-download). These scripts require the appropriate templates which can be downloaded from the Juna. Chimp web viewer (SPM/CAT_templates.zip) and then place the templates_animals/ folder into the latest version CAT12 Toolbox directory (CAT12.7 r1609). The processing parameters are similar to those conducted in this study, although different DICOM conversions and denoising were conducted. Further information regarding each parameter can be viewed when opening the script in the SPM batch as well as the provided comments and README file. The code for the workflow in addition to the code used to conduct the aging effect and asymmetry analyses can be found here https://github.com/viko18/JunaChimp.

Acknowledgements

548	We would like to thank Jona Fischer for the creation of the interactive Juna. Chimp
549	web viewer adapted from nehuba (github).
550	
551	References
552	Alexander GE, Chen K, Aschenbrenner M, Merkley TL, Santerre-Lemmon LE, Shamy
553	JL, Skaggs WE, Buonocore MH, Rapp PR, Barnes CA. 2008. Age-related regional
554	network of magnetic resonance imaging gray matter in the rhesus macaque. J
555	Neurosci. 28:2710–2718.
556	Amunts K, Schleicher A, Bürgel U, Mohlberg H, Uylings HBM, Zilles K. 1999. Broca's
557	region revisited: Cytoarchitecture and intersubject variability. J Comp Neurol.
558	412:319–341.
559	Amunts K, Zilles K. 2015. Architectonic Mapping of the Human Brain beyond Brodmann.
560	Neuron.
561	Anderson JR, Gallup GG. 2015. Mirror self-recognition: a review and critique of
562	attempts to promote and engineer self-recognition in primates. Primates. 56:317-
563	326.
564	Ashburner J, Friston KJ. 2000. Voxel-based morphometrythe methods. Neuroimage.
565	11:805–821.
566	Ashburner J, Friston KJ. 2005. Unified segmentation. Neuroimage. 26:839–851.
567	Ashburner J, Friston KJ. 2011. Diffeomorphic registration using geodesic shooting and
568	Gauss-Newton optimisation. Neuroimage. 55:954–967.
569	Autrey MM, Reamer LA, Mareno MC, Sherwood CC, Herndon JG, Preuss T, Schapiro
570	SJ, Hopkins WD. 2014. Age-related effects in the neocortical organization of
571	chimpanzees: gray and white matter volume, cortical thickness, and gyrification.
572	Neuroimage. 101:59–67.
573	Bailey P, Bonin GV MW. 1950. The isocortex of the chimpanzee. Urbana, IL: Univ of
574	Illinois Press.
575	Bard KA, Hopkins WD. 2018. Early Socioemotional Intervention Mediates Long-Term
576	Effects of Atypical Rearing on Structural Covariation in Gray Matter in Adult
577	Chimpanzees. Psychol Sci. 29:594–603.
578	Bogart SL, Bennett AJ, Schapiro SJ, Reamer LA, Hopkins WD. 2014. Different early

579 rearing experiences have long term effects on cortical organization in captive 580 chimpanzees (Pan troglodytes). Dev Sci. 17:161–174. 581 Bogart SL, Mangin JF, Schapiro SJ, Reamer L, Bennett AJ, Pierre PJ, Hopkins WD. 582 2012. Cortical sulci asymmetries in chimpanzees and macagues: A new look at an 583 old idea. Neuroimage. 61:533-541. 584 Chen X, Errangi B, Li L, Glasser MF, Westlye LT, Fjell AM, Walhovd KB, Hu X, Herndon 585 JG, Preuss TM, Rilling JK. 2013. Brain aging in humans, chimpanzees (Pan 586 troglodytes), and rhesus macaques (Macaca mulatta): magnetic resonance imaging 587 studies of macro- and microstructural changes. Neurobiol Aging. 34:2248–2260. 588 Chiarello C, Vazquez D, Felton A, McDowell A. 2016. Structural asymmetry of the 589 human cerebral cortex: Regional and between-subject variability of surface area, 590 cortical thickness, and local gyrification. Neuropsychologia. 93:365–379. 591 Crivello F, Tzourio-Mazoyer N, Tzourio C, Mazoyer B. 2014. Longitudinal assessment of 592 global and regional rate of grey matter atrophy in 1,172 healthy older adults: 593 Modulation by sex and age. PLoS One. 9. 594 Dahl CD, Adachi I. 2013. Conceptual metaphorical mapping in chimpanzees (Pan 595 troglodytes). Elife. 2013. 596 Dahnke R, Gaser C. 2017. Voxel-based Preprocessing in CAT. Organ Hum Brain 597 Марр. 598 Dahnke R, Ziegler G, Gaser C. 2012. Local Adaptive Segmentation. Hum Brain Mapp 599 Conf. 600 Emery Thompson M, Fox SA, Berghänel A, Sabbi KH, Phillips-Garcia S, Enigk DK, Otali 601 E, Machanda ZP, Wrangham RW, Muller MN. 2020. Wild chimpanzees exhibit 602 humanlike aging of glucocorticoid regulation. Proc Natl Acad Sci. 201920593. 603 Franke K, Clarke GD, Dahnke R, Gaser C, Kuo AH, Li C, Schwab M, Nathanielsz PW. 604 2017. Premature Brain Aging in Baboons Resulting from Moderate Fetal 605 Undernutrition. Front Aging Neurosci. 9:92. 606 Freeman HD, Cantalupo C, Hopkins WD. 2004. Asymmetries in the hippocampus and 607 amygdala of chimpanzees (Pan troglodytes). Behav Neurosci. 118:1460–1465. 608 Gannon PJ, Holloway RL, Broadfield DC, Braun AR. 1998. Asymmetry of chimpanzee

planum temporale: Humanlike pattern of Wernicke's brain language area homolog.

- 610 Science (80-). 279:220–222.
- Gaser C, Dahnke R, Kurth K, Luders E, Alzheimer's Disease Neuroimaging Initiative.
- 612 2020. A computational Anatomy Toolbox for the Analysis of Structural MRI Data.
- 613 Neuroimage.
- Gilissen EP, Hopkins WD. 2013. Asymmetries of the parietal operculum in chimpanzees
- (Pan troglodytes) in relation to handedness for tool use. Cereb Cortex. 23:411–422.
- 616 Gomez-Robles A, Hopkins WD, Sherwood CC. 2013. Increased morphological
- asymmetry, evolvability and plasticity in human brain evolution. Proc Biol Sci.
- 618 280:20130575.
- 619 Good CD, Johnsrude I, Ashburner J, Henson RNA, Friston KJ, Frackowiak RSJ. 2001a.
- 620 Cerebral asymmetry and the effects of sex and handedness on brain structure: A
- voxel-based morphometric analysis of 465 normal adult human brains.
- 622 Neuroimage. 14:685–700.
- 623 Good CD, Johnsrude IS, Ashburner J, Henson RN, Friston KJ, Frackowiak RS. 2001b.
- A voxel-based morphometric study of ageing in 465 normal adult human brains.
- 625 Neuroimage. 14:21–36.
- Hecht EE, Mahovetz LM, Preuss TM, Hopkins WD. 2017. A neuroanatomical predictor
- of mirror self-recognition in chimpanzees. Soc Cogn Affect Neurosci. 12:37–48.
- Herndon JG, Tigges J, Anderson DC, Klumpp SA, McClure HM. 1999. Brain weight
- throughout the life span of the chimpanzee. J Comp Neurol. 409:567–572.
- Holm S. 1979. A Simple Sequentially Rejective Multiple Test Procedure. Scand J Stat.
- 631 6:65–70.
- Hopkins WD, Avants BB. 2013. Regional and hemispheric variation in cortical thickness
- in chimpanzees (Pan troglodytes). J Neurosci. 33:5241–5248.
- Hopkins WD, Cantalupo C. 2004. Handedness in chimpanzees (Pan troglodytes) is
- associated with asymmetries of the primary motor cortex but not with homologous
- language areas. Behav Neurosci. 118:1176–1183.
- Hopkins WD, Cantalupo C, Taglialatela J. 2007. Handedness Is Associated with
- Asymmetries in Gyrification of the Cerebral Cortex of Chimpanzees. Cereb Cortex.
- 639 17:1750–1756.
- Hopkins WD, Li X, Crow T, Roberts N. 2017. Vertex- and atlas-based comparisons in

641 measures of cortical thickness, gyrification and white matter volume between 642 humans and chimpanzees. Brain Struct Funct. 222:229-245. 643 Hopkins WD, Meguerditchian A, Coulon O, Bogart S, Mangin JF, Sherwood CC, Grabowski MW, Bennett AJ, Pierre PJ, Fears S, Woods R, Hof PR, Vauclair J. 644 645 2014a. Evolution of the central sulcus morphology in primates. Brain Behav Evol. 646 84:19-30. 647 Hopkins WD, Meguerditchian A, Coulon O, Bogart S, Mangin JF, Sherwood CC, 648 Grabowski MW, Bennett AJ, Pierre PJ, Fears S, Woods R, Hof PR, Vauclair J. 649 2014b. Evolution of the Central Sulcus Morphology in Primates. Brain Behav Evol. 650 84:19-30. 651 Hopkins WD, Misiura M, Pope SM, Latash EM. 2015. Behavioral and brain asymmetries 652 in primates: A preliminary evaluation of two evolutionary hypotheses. Ann N Y Acad 653 Sci. 1359:65-83. 654 Hopkins WD, Nir TM. 2010. Planum temporale surface area and grey matter 655 asymmetries in chimpanzees (Pan troglodytes): The effect of handedness and 656 comparison with findings in humans. Behav Brain Res. 208:436–443. 657 Hopkins WD, Taglialatela JP, Meguerditchian A, Nir T, Schenker NM, Sherwood CC. 658 2008. Gray matter asymmetries in chimpanzees as revealed by voxel-based 659 morphometry. Neuroimage. 42:491–497. 660 Jagust W. 2016. Is amyloid-β harmful to the brain? Insights from human imaging 661 studies. Brain. 139:23-30. 662 Jagust W. 2018. Imaging the evolution and pathophysiology of Alzheimer disease. Nat 663 Rev Neurosci. 664 Keller SS, Roberts N, Hopkins W. 2009. A Comparative Magnetic Resonance Imaging 665 Study of the Anatomy, Variability, and Asymmetry of Broca's Area in the Human and Chimpanzee Brain. J Neurosci. 29:14607-14616. 666 667 Kennedy KM, Erickson KI, Rodrigue KM, Voss MW, Colcombe SJ, Kramer AF, Acker 668 JD, Raz N. 2009. Age-related differences in regional brain volumes: A comparison

26

of optimized voxel-based morphometry to manual volumetry. Neurobiol Aging.

Koelkebeck K, Miyata J, Kubota M, Kohl W, Son S, Fukuyama H, Sawamoto N,

669

670

671

30:1657-1676.

673 to gray matter asymmetries in the healthy human brain. Hum Brain Mapp. 35:6011-674 6022. 675 Kong XZ, Mathias SR, Guadalupe T, Abé C, Agartz I, Akudjedu TN, Aleman A, 676 Alhusaini S, Allen NB, Ames D, Andreassen OA, Vasquez AA, Armstrong NJ, 677 Bergo F, Bastin ME, Batalla A, Bauer J, Baune BT, Baur-Streubel R, Biederman J, 678 Blaine SK, Boedhoe P, Bøen E, Bose A, Bralten J, Brandeis D, Brem S, Brodaty H, 679 Yüksel D, Brooks SJ, Buitelaar J, Bürger C, Bülow R, Calhoun V, Calvo A, 680 Canales-Rodríguez EJ, Canive JM, Cannon DM, Caparelli EC, Castellanos FX, 681 Cavalleri GL, Cendes F, Chaim-Avancini TM, Chantiluke K, Chen QL, Chen X, 682 Cheng Y, Christakou A, Clark VP, Coghill D, Connolly CG, Conzelmann A, 683 Córdova-Palomera A, Cousiin J, Crow T, Cubillo A, Dale A, Dannlowski U, De 684 Bruttopilo SA, De Zeeuw P, Deary IJ, Delanty N, Demeter D V., Di Martino A, 685 Dickie EW, Dietsche B, Doan NT, Doherty CP, Doyle A, Durston S, Earl E, Ehrlich 686 S, Ekman CJ, Elvsåshagen T, Epstein JN, Fair DA, Faraone S V., Fernández G, 687 Filho GB, Förster K, Fouche JP, Foxe JJ, Frodl T, Fuentes-Claramonte P, Fullerton 688 J, Garavan H, Garcia DDS, Gotlib IH, Goudriaan AE, Grabe HJ, Groenewold NA, 689 Grotegerd D, Gruber O, Gurholt T, Haavik J, Hahn T, Hansell NK, Harris MA, 690 Hartman CA, Hernández MDCV, Heslenfeld D, Hester R, Hibar DP, Ho BC, Ho TC, 691 Hoekstra PJ, Van Holst RJ, Hoogman M, Høvik MF, Howells FM, Hugdahl K, 692 Huyser C, Ingvar M, Irwin L, Ishikawa A, James A, Jahanshad N, Jernigan TL, 693 Jönsson EG, Kähler C, Kaleda V, Kelly C, Kerich M, Keshavan MS, Khadka S, 694 Kircher T, Kohls G, Konrad K, Korucuoglu O, Krämer B, Krug A, Kwon JS, 695 Lambregts-Rommelse N, Landén M, Lázaro L, Lebedeva I, Lenroot R, Lesch KP, Li 696 Q, Lim KO, Liu J, Lochner C, London ED, Lonning V, Lorenzetti V, Luciano M, 697 Luijten M, Lundervold AJ, MacKey S, MacMaster FP, Maingault S, Malpas CB, Malt 698 UF, Mataix-Cols D, Martin-Santos R, Mayer AR, McCarthy H, Mitchell PB, Mueller 699 BA, Maniega SM, Mazoyer B, McDonald C, McLellan Q, McMahon KL, McPhilemy

Takahashi H, Murai T. 2014. The contribution of cortical thickness and surface area

672

700

701

702

G, Momenan R, Morales AM, Narayanaswamy JC, Moreira JCV, Nerland S, Nestor

Oosterlaan J, Oranje B, Orr C, Overs B, Pauli P, Paulus M, Plessen KJ, Von Polier

L, Newman E, Nigg JT, Nordvik JE, Novotny S, Weiss EO, O'Gorman RL,

- GG, Pomarol-Clotet E, Portella MJ, Qiu J, Radua J, Ramos-Quiroga JA, Reddy
- YCJ, Reif A, Roberts G, Rosa P, Rubia K, Sacchet MD, Sachdev PS, Salvador R,
- Schmaal L, Schulte-Rüther M, Schweren L, Seidman L, Seitz J, Serpa MH, Shaw
- P, Shumskaya E, Silk TJ, Simmons AN, Simulionyte E, Sinha R, Sjoerds Z,
- Smelror RE, Soliva JC, Solowij N, Souza-Duran FL, Sponheim SR, Stein DJ, Stein
- EA, Stevens M, Strike LT, Sudre G, Sui J, Tamm L, Temmingh HS, Thoma RJ,
- Tomyshev A, Tronchin G, Turner J, Uhlmann A, Van Erp TGM, Van Den Heuvel
- OA, Van Der Meer D, Van Eijk L, Vance A, Veer IM, Veltman DJ,
- Venkatasubramanian G, Vilarroya O, Vives-Gilabert Y, Voineskos AN, Völzke H,
- Vuletic D, Walitza S, Walter H, Walton E, Wardlaw JM, Wen W, Westlye LT,
- Whelan CD, White T, Wiers RW, Wright MJ, Wittfeld K, Yang TT, Yasuda CL,
- Yoncheva Y, Yücel M, Yun JY, Zanetti MV, Zhen Z, Zhu XX, Ziegler GC, Zierhut K,
- De Zubicaray GI, Zwiers M, Glahn DC, Franke B, Crivello F, Tzourio-Mazoyer N,
- Fisher SE, Thompson PM, Francks C, Farde L, Flyckt L, Engberg G, Erhardt S,
- Fatouros-Bergman H, Cervenka S, Schwieler L, Piehl F, Collste K, Victorsson P,
- 718 Malmqvist A, Hedberg M, Orhan F. 2018. Mapping cortical brain asymmetry in
- 719 17,141 healthy individuals worldwide via the ENIGMA consortium. Proc Natl Acad
- 720 Sci U S A. 115:E5154–E5163.
- 721 Kurth F, Gaser C, Luders E. 2015. A 12-step user guide for analyzing voxel-wise gray
- matter asymmetries in statistical parametric mapping (SPM). Nat Protoc. 10:293–
- 723 304.
- La Joie R, Perrotin A, Barre L, Hommet C, Mezenge F, Ibazizene M, Camus V, Abbas
- A, Landeau B, Guilloteau D, de La Sayette V, Eustache F, Desgranges B, Chetelat
- G. 2012. Region-specific hierarchy between atrophy, hypometabolism, and beta-
- amyloid (Abeta) load in Alzheimer's disease dementia. J Neurosci. 32:16265-
- 728 **16273**.
- Langergraber KE, Prüfer K, Rowney C, Boesch C, Crockford C, Fawcett K, Inoue E,
- 730 Inoue-Muruyama M, Mitani JC, Muller MN, Robbins MM, Schubert G, Stoinski TS,
- Viola B, Watts D, Wittig RM, Wrangham RW, Zuberbuhler K, Pääbo S, Vigilant L.
- 732 2012. Generation times in wild chimpanzees and gorillas suggest earlier
- divergence times in great ape and human evolution. Proc Natl Acad Sci U S A.

- 734 109:15716–15721.
- Li X, Crow TJ, Hopkins WD, Gong Q, Roberts N. 2018. Human torque is not present in
- chimpanzee brain. Neuroimage. 165:285–293.
- 137 Llado A, Tort-Merino A, Sanchez-Valle R, Falgas N, Balasa M, Bosch B, Castellvi M,
- Olives J, Antonell A, Hornberger M. 2018. The hippocampal longitudinal axis-
- relevance for underlying tau and TDP-43 pathology. Neurobiol Aging. 70:1–9.
- Luders E, Narr KL, Thompson PM, Rex DE, Jancke L, Toga AW. 2006. Hemispheric
- asymmetries in cortical thickness. Cereb Cortex. 16:1232–1238.
- Lyn H, Pierre P, Bennett AJ, Fears S, Woods R, Hopkins WD. 2011. Planum temporale
- grey matter asymmetries in chimpanzees (Pan troglodytes), vervet (Chlorocebus
- aethiops sabaeus), rhesus (Macaca mulatta) and bonnet (Macaca radiata)
- monkeys. Neuropsychologia. 49:2004–2012.
- Mai JK, Majtanik M, Paxinos G. 2015. Atlas of the Human Brain. Elsevier Science.
- Maingault S, Tzourio-Mazoyer N, Mazoyer B, Crivello F. 2016. Regional correlations
- 548 between cortical thickness and surface area asymmetries: A surface-based
- morphometry study of 250 adults. Neuropsychologia. 93:350–364.
- 750 Manjon J V, Coupe P, Marti-Bonmati L, Collins DL, Robles M. 2010. Adaptive non-local
- means denoising of MR images with spatially varying noise levels. J Magn Reson
- 752 Imaging. 31:192–203.
- Marie D, Roth M, Lacoste R, Nazarian B, Bertello A, Anton JL, Hopkins WD,
- Margiotoudi K, Love SA, Meguerditchian A. 2018. Left Brain Asymmetry of the
- 755 Planum Temporale in a Nonhominid Primate: Redefining the Origin of Brain
- 756 Specialization for Language. Cereb Cortex. 28:1808–1815.
- 757 Mazziotta J, Toga A, Evans A, Fox P, Lancaster J, Zilles K, Woods R, Paus T, Simpson
- G, Pike B, Holmes C, Collins L, Thompson P, MacDonald D, Iacoboni M,
- Schormann T, Amunts K, Palomero-Gallagher N, Geyer S, Parsons L, Narr K,
- Kabani N, Le Goualher G, Boomsma D, Cannon T, Kawashima R, Mazoyer B.
- 761 2001. A probabilistic atlas and reference system for the human brain: International
- Consortium for Brain Mapping (ICBM). Philos Trans R Soc B Biol Sci.
- Minkova L, Habich A, Peter J, Kaller CP, Eickhoff SB, Klöppel S. 2017. Gray matter
- asymmetries in aging and neurodegeneration: A review and meta-analysis. Hum

- 765 Brain Mapp. 38:5890–5904.
- Plessen KJ, Hugdahl K, Bansal R, Hao X, Peterson BS. 2014. Sex, age, and cognitive
- correlates of asymmetries in thickness of the cortical mantle across the life span. J
- 768 Neurosci. 34:6294–6302.
- Rajapakse JC, Giedd JN, Rapoport JL. 1997. Statistical approach to segmentation of
- single-channel cerebral mr images. IEEE Trans Med Imaging. 16:176–186.
- 771 Rilling JK, Insel TR. 1999. The primate neocortex in comparative perspective using
- magnetic resonance imaging. J Hum Evol. 37:191–223.
- Rorder C, Brett M. 2000. Stereotaxic Display of Brain Lesions. Behav Neurol. 12.
- Savage-Rumbaugh ES. 1986. Ape language: from conditioned response to symbol.
- 775 Oxford University Press.
- Savage-Rumbaugh ES, Lewin R. 1994. Kanzi: the ape at the brink of the human mind.
- 777 Wiley.
- Schenker NM, Hopkins WD, Spocter MA, Garrison AR, Stimpson CD, Erwin JM, Hof
- PR, Sherwood CC. 2010. Broca's Area Homologue in Chimpanzees (Pan
- troglodytes): Probabilistic Mapping, Asymmetry, and Comparison to Humans.
- 781 Cereb Cortex. 20:730–742.
- 782 Shamy JL, Habeck C, Hof PR, Amaral DG, Fong SG, Buonocore MH, Stern Y, Barnes
- CA, Rapp PR. 2011. Volumetric correlates of spatiotemporal working and
- recognition memory impairment in aged rhesus monkeys. Cereb Cortex. 21:1559–
- 785 **1573**.
- Sherwood CC, Broadfield DC, Holloway RL, Gannon PJ, Hof PR. 2003. Variability of
- Broca's area homologue in African great apes: Implications for language evolution.
- 788 Anat Rec Part A Discov Mol Cell Evol Biol. 271:276–285.
- Sherwood CC, Gordon AD, Allen JS, Phillips KA, Erwin JM, Hof PR, Hopkins WD. 2011.
- Aging of the cerebral cortex differs between humans and chimpanzees. Proc Natl
- 791 Acad Sci U S A. 108:13029–13034.
- 792 Shumaker RW, Walkup KR, Beck BB. 2011. Animal tool behavior: the use and
- manufacture of tools by animals. Johns Hopkins University Press.
- 794 Smith SM, Nichols TE. 2009. Threshold-free cluster enhancement: Addressing
- 795 problems of smoothing, threshold dependence and localisation in cluster inference.

796	Neuroimage. 44:83–98.
797	Spocter MA, Hopkins WD, Garrison AR, Bauernfeind AL, Stimpson CD, Hof PR,
798	Sherwood CC. 2010. Wernicke's area homologue in chimpanzees IPan troglodytes
799	and its relation to the appearance of modern human language. Proc R Soc B Biol
800	Sci. 277:2165–2174.
801	Taglialatela JP, Cantalupo C, Hopkins WD. 2006. Gesture handedness predicts
802	asymmetry in the chimpanzee inferior frontal gyrus. Neuroreport. 17:923–927.
803	Toga AW, Thompson PM. 2003. Mapping brain asymmetry. Nat Rev Neurosci. 4:37–48.
804	Tohka J, Zijdenbos A, Evans A. 2004. Fast and robust parameter estimation for
805	statistical partial volume models in brain MRI. Neuroimage. 23:84–97.
806	Tomasello M, Call J. 1997. Primate Cognition.
807	Uylings HBM, Jacobsen AM, Zilles K, Amunts K. 2006. Left-right asymmetry in volume
808	and number of neurons in adult Broca's area. Cortex. 42:652–658.
809	Waal FBM de (Frans BM. 1996. Good natured : the origins of right and wrong in humans
810	and other animals. Harvard University Press.
811	Waterson RH, Lander ES, Wilson RK. 2005. Initial sequence of the chimpanzee
812	genome and comparison with the human genome. Nature. 437:69–87.
813	Watkins KE. 2001. Structural Asymmetries in the Human Brain: a Voxel-based
814	Statistical Analysis of 142 MRI Scans. Cereb Cortex. 11:868–877.
815	Xiang L, Crow T, Roberts N. 2019. Cerebral torque is human specific and unrelated to
816	brain size. Brain Struct Funct. 224:1141–1150.
817	Zhou D, Lebel C, Evans A, Beaulieu C. 2013. Cortical thickness asymmetry from
818	childhood to older adulthood. Neuroimage. 83:66–74.
819	Zilles K, Armstrong E, Moser KH, Schleicher A, Stephan H. 1989. Gyrification in the
820	cerebral cortex of primates. Brain Behav Evol. 34:143–150.
821	Zilles K, Dabringhaus A, Geyer S, Amunts K, Qü M, Schleicher A, Gilissen E, Schlaug
822	G, Steinmetz H. 1996. Structural asymmetries in the human forebrain and the
823	forebrain of non- human primates and rats. In: Neuroscience and Biobehavioral
824	Reviews. Elsevier Ltd. p. 593–605.
825	

Ethics

The chimpanzee imaging data was acquired under protocols approved by the
Yerkes National Primate Research Center (YNPRC) at Emory University Institutional An-
imal Care and Use Committee (Approval number YER2001206).
Supplementary and Source Data Files
Figure 2 – source data 1: Source file for Complete List of Davi130 Labels
• Figure 3 – supplement 1: Age and sex distribution of complete chimpanzee (223)
sample separated by scanner strength.
 Figure 4 – source data 1: Aging Effect on Gray Matter in Complete Davi130 Labels Figure 6 – source data 1: Complete Davi130 labels hemispheric asymmetry